Synthesis of nc-UO$_2$ by controlled precipitation in aqueous phase
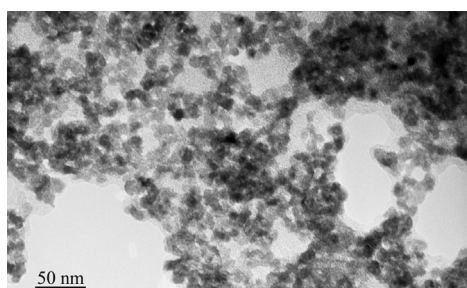
R. Jovani-Abril [a], *, M. Gibilaro [b], A. Janßen [a], R. Eloirdi [a], J. Somers [a], J. Spino [a], R. Malmbeck [a]

[a] European Commission, Joint Research Centre, Institute for Transuranium Elements, P.O.Box 2340, D-76125 Karlsruhe, Germany
[b] Laboratoire de Génie Chimique (LGC), Université de Toulouse, UMR CNRS 5503, 31062 Toulouse cedex 9, France

GRAPHICAL ABSTRACT

50 nm

ARTICLE INFO

ABSTRACT

Nanocrystalline UO$_2$ has been produced through controlled precipitation from an electrolytically reduced U(IV) solution. The reduction process of U(VI) to U(IV) was investigated by cyclic voltammetry in combination with absorption spectrophotometry. Precipitation was achieved by controlled alkalinisation following closely the solubility line of U(IV) in aqueous media. The highest starting concentration used was 0.5 M uranylnitrate which yielded, with the equipment used, around 10 g material pro batch. The produced nc-UO$_2$ was characterised by transmission electron microscopy (TEM) and x-ray diffraction (XRD) and exhibited the typical UO$_{2+x}$ fcc fluorite structure with an average crystallite size of 3.9 nm.

© 2016 Elsevier B.V. All rights reserved.

1. Introduction

Today's nuclear fuels are largely based on uranium dioxide (UO$_2$). A high level of proficiency has been reached in this technology with fuels achieving moderate to high burn-up (BU) in the reactor. Even higher BU's are desirable to provide more efficient fuel utilisation and, thereby, a reduction of the amount of fresh fuel and the mass of spent fuel inventories (radioactive waste). To reach higher BU's an improved fission gas retention capability of the fuel is required as well as a solution to the pellet clad mechanical and chemical interaction (PCMI and PCCI) failure risks [1,2]. This is a problem, which could intensify at high BUs due to boosted cladding embrittlement. It has been demonstrated that the nanocrystalline (nc) phase formed at the rim of the fuel by restructuring at very high BUs, the so called High Burn-up Structure (HBS) [3,4], has exceptional qualities with a number of improved and advantageous

* Corresponding author.
E-mail address: raqueljovaniabril@gmail.com (R. Jovani-Abril).

properties for the fuel. Among these are a closed porosity [5–7], improvement of mechanical properties such as plasticity and creep strain [8,9] and an improved resistance against radiation damage [10]. Thus, the manufacturing of a bulk nc-fuel with a structure resembling that of the HBS phase has been proposed as a radical approach to improve fuel performance [10]. The starting material for any nc-fuel compound is, however, a well characterised nc-UO_2 powder, synthesised and made available in a quantity large enough to produce a compact or pellet. Although much information can be found about nano-chemistry and actinide chemistry, information on the synthesis of nanoparticles with actinides is up to now rather scarce. The few studies reported are concerned with the issue of radionuclide release through nanosized colloids from a spent fuel geological repository [11–14]. In a few other cases, the synthesis of high quality nanostructures based on uranium dioxides have been motivated for catalytical purposes [15] or to study possible size dependent physical and chemical properties [16,17]. The synthesis methods can generally be divided into organometallic decomposition or aqueous methods, the latter based on precipitation of nc-UO_2 from U(IV) solutions [18]. Despite that, no publications, including those referenced above, describe the production of nc-actinides other than for very small quantities needed for analytical purposes. This work aims to design a method suitable for larger scale production of nc-UO_2 by improving and scaling up existing synthesis methods based on precipitation in aqueous media. A full characterisation of the produced material has been performed.

1.1. U-stability in aqueous solution

The calculated equilibrium solubility lines of U(IV) and U(VI) species in aqueous solution as a function of pH have been reported by Neck and Fanghänel, [19,20]. In Fig. 1 a plot of these results as compiled by Gil et al. [18] is shown. There are several orders of magnitude between the solubility of U(IV) in presence of its crystalline dioxide phase $UO_2(c)$, or in presence of the amorphous form of this phase (hydrated uraninite $UO_2 \cdot xH_2O(am)$. Also several orders of magnitude separate the latter compounds with the solubility line of U(VI) in presence of the crystalline hydroxide phase schoepite, $UO_2(OH)_2(s)$ [18]. Valuable experimental data of the oxidation state of uranium in the precipitates and the size of their corresponding agglomerates, along the solubility line have been reported at different pH and low U concentrations [11,21–23]. They show a two-fold behaviour, matching that of crystalline $UO_2(c)$ with 8–13 nm size at pH values around 1 and that of the amorphous hydrated phase (with 80–150 nm size) at pH > 2.5, which indicates also the onset of hydrolysis of U(IV) in solution [19]. One can conclude from Fig. 1, that by provoking precipitation close to the U(IV) solubility line at low pH, the smallest and the more crystalline form of the precipitates can be obtained and at the same time avoiding, or at least minimizing, the co-precipitation of any amorphous hydroxide uranium form. Previous experience, has shown the synthesis of nc-material using this method can yield only small quantities of the material along with undesirable large quantities of waste. The use of higher uranium concentrations and their correspondingly lower precipitation range was already suggested but not tested by Opel et al. [11]. In their perchlorate system these authors proposed moving the U(IV)-precipitation line towards lower pHs, as a means to obtain nano-UO_2 precipitates in its crystalline form and simultaneously diminishing the size of the agglomerates. In this work, a similar concept has been followed. A study of the range of U-concentration and acidity for UO_{2+x} precipitation from electrolytically reduced uranyl nitrate $UO_2(NO_3)_2$ has been carried out and the obtained precipitates characterised in terms of agglomerate size and crystallinity.

2. Experimental

2.1. Solutions and reagents

A U(VI) stock solution was prepared by dissolving yellow uranylnitrate $UO_2(NO_3)_2$ powder in deionised water (18.2 MΩ/cm) by continuous stirring at 80 °C, to a concentration of 500 gU/l. This solution was further diluted into a 1 M NaCl or 1 M HCl (Alfa Aesar, p.A grade) solution to a uranium concentration range of 0.02–0.5 M. 1 M HCl was used to avoid hydrolysis in the more concentrated U solutions. Adjustments of pH were made by adding 1 M HCl or 1 M NaOH (Alfa Aesar) solutions. For measurement of pH a standard pH glass electrode was used in combination with a pH meter.

2.2. Experimental set-up and electrochemical techniques

The experiments were all carried out in glove boxes under N_2 atmosphere (O_2 ~ 0.5%) and under constant bubbling of inert Ar gas (99.99%) into the reactor and the solutions. Electrochemical techniques, i.e. cyclic voltammetry (CV) and potentiostatic electrolysis were carried out with a SP5-50 potentiostat from BioLogic Science Instruments (working range + −10 V, 800 mA). The set-up (see Fig. 2) was a 150 mL glass reactor with a 5 necked glass lid designed to hold and position the electrodes, with inlets and outlets for gas. It was placed on a hot plate with magnetic stirrer. A Teflon® magnet bar in combination with constant Ar gas bubbling was used to stir and homogenise the solution during the experiments. The Ar gas flow was temporarily stopped during electrochemical measurements to ensure stable signals. All experiments were performed at room temperature. In Fig. 2 a typical set-up used for the reduction and controlled precipitation, is shown.

The electrochemical behaviour of uranium was characterised by cyclic voltammetry using a three electrode set-up consisting of a Pt/Ir (90%/10%) electrodes and a standard reference electrode. The working electrode was a 1 mm diameter rod in spiral form having an active surface area of about 1.9 cm². The counter electrode (Heraeus, Fischer type, El 04) was a large surface cylindrical 0.12 mm mesh sized net anode (dimensions; 38 mm diameter, 50 mm height and 0.12 mm wire thickness). The reference electrode used was an Ag/AgCl/Cl⁻ saturated Inlab® Reference electrode obtained from Mettler Toledo. Before the begin of an experimental series the pH of the solution was measured and adjusted to the desired value. New solutions were prepared for each CV study between which the electrodes were carefully cleaned.

For the reduction of U(VI) to U(IV), electrolysis at constant potential was carried out using the same electrochemical set-up but with the large surface cylindrical net as cathode and the spiral electrode as anode. In order to prevent oxygen formed in the anodic reaction, to enter the reaction vessel, the anode was introduced in a separate glass tube with ionic connection to the surrounding solution established through a permeable glass frit (160 μm porosity). The anodic compartment was filled with 1 M HCl. The cell reactions during electrochemical reduction of U(VI) to U(IV) are Eq. (1) for the cathode and Eq. (2) for the anode, respectively.

$$UO_2^{2+} + 4H^+ + 2e^- \leftrightarrow U^{4+} + 2H_2O \tag{1}$$

$$2H_2O \leftrightarrow 4H^+ + 4e^- + O_2 \tag{2}$$
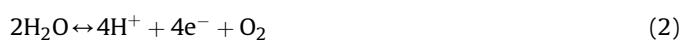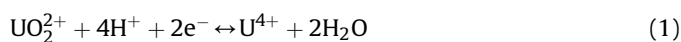
Due to the anodic reaction, continuous stirring and bubbling of the solution with oxygen free Ar gas to remove oxygen was applied, which also reinforced the homogenisation of the solution during electrolysis. The electrolysis was continuously monitored by
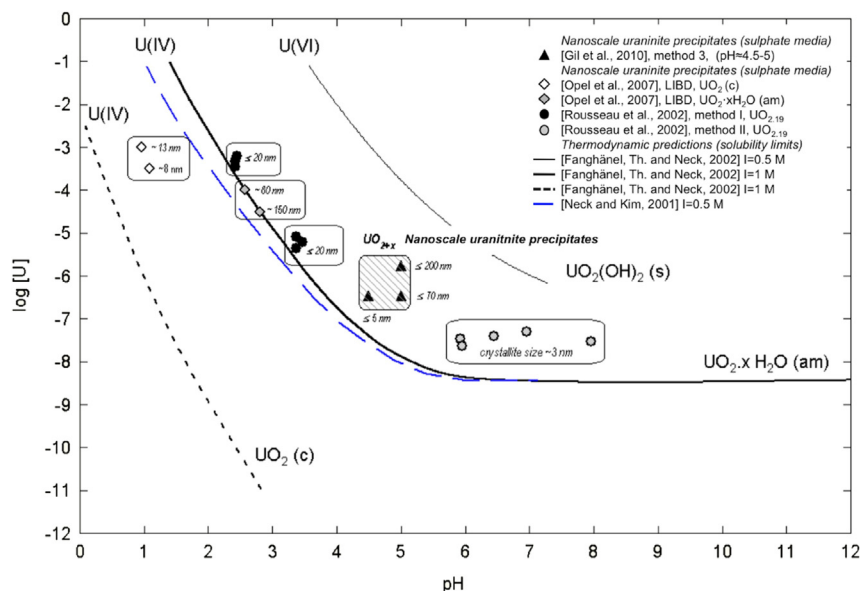
Fig. 1. Theoretical solubility limits of U(IV) and U(VI) species in aqueous solutions [19,20] and experimental determinations for uranium sulphate [18] and uranium chloride [11,12]. Compounds shown beside each solubility line represent the precipitated solid phase when these conditions are exceeded [24].
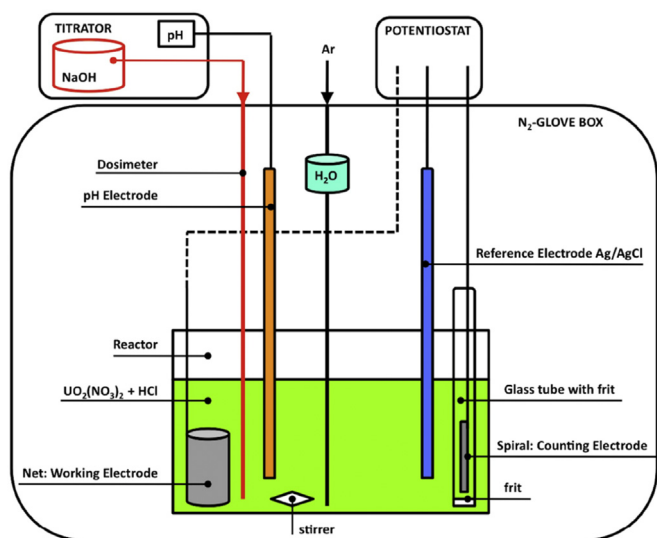

Fig. 2. Experimental set-up used for electrochemistry and precipitation of nc-UO$_2$ [24].

recording the current versus the time. During electrolysis the uranium solution was periodically sampled and the U(IV)/U(VI) ratio controlled by UV-Vis spectrophotometry (Lambda 9, Perkin Elmer). Occasionally the electrolysis was stopped and cyclic voltammetry was performed to investigate the U(VI)/U(IV) reduction peak. By these methods the progress of the reduction process could be monitored and investigated. The reduction process yielded a fluorescent green U(IV) solution with a pH around 0.5.

2.3. Synthesis of nc-UO$_{2+x}$

Precipitation of UO$_2$ from electrochemically reduced U(IV) solutions, in the same experimental set-up, was achieved by slow, gradual and controlled alkalinisation of the solution using a titrator (Metrohm Titrando 906) with pH control (iEcotrode Plus Metrohm). The starting pH was normally around 0.5 and 3 M NaOH was titrated to the solution at a rate of 10–20 μL/min. The slow alkalinisation was automatically stopped when the solution reached a desired pH value and restarted again as the pH dropped due to the precipitation reaction (Eq. (3)).

$$U^{4+} + 4OH^- \leftrightarrow UO_2(c) + 2H_2O \qquad (3)$$

Ar bubbling and continuous stirring was applied during the precipitation reaction but without an applied redox potentiometric control. During precipitation the evolution of pH was continuously monitored against time (and added base), in addition samples were taken for UV-Vis spectrophotometry of U(IV). The precipitates were separated by centrifugation at 3500 rpm (RCF = 2205 g) during 30 min (Eppendorf centrifuge 5804; Swing-bucket rotor A-4-44) and the supernatant liquid was discarded. In order to remove Na$^+$ and Cl$^-$ impurities, the precipitates were further washed 5 times with about 40 mL deionised water to 1.25 g solids.

2.3.1. Characterisation of nc-UO$_{2+x}$

The morphology and dimensions of the nc-UO$_{2+x}$ samples were investigated by high resolution transmission electron microscopy, HRTEM (200 kV FEI Tecnai G2 F20 XT), equipped with a Gatan US 1000 CCD camera for TEM imaging. The samples for TEM imaging were prepared, outside the nitrogen glovebox in air, by suspending the solid particles in ethanol in an ultrasonic bath. A drop of the well dispersed solution was loaded on a carbon coated 200 mesh copper grid, which was dried under ambient conditions, before the grid was placed on the sample holder of the microscope.

The crystal structure and crystallite size were investigated by XRD using a θ–2θ diffractometer (D8, Advance, Bruker AXS) operating with a Ge(111) monochromator and a Cu-Kα$_1$ source and the 1-dimensional detector LynxEye. XRD patterns were recorded in the 2θ range 20°–120° with a step size of 0.01° and a counting time of 5 s per step. Rietveld refinement was performed using X'Pert Highscore Plus version 3.0d software with the help of ICDD (International Centre for Diffraction Data) database, PDF-4+ (powder diffraction file) release 2013. The samples were loaded (about 50 mg) on a flat specimen holder of Si-911 crystal providing a low background.

3. Results and discussion

Fig. 3 shows a typical result from cyclic voltammetry of UO_2^{2+} solutions. The electrochemical window is set by the stability of the solvent from -1.0 V (reduction, see Eq. (4)) to $+1.2$ V (oxidation, see Eq. (5)) vs Ag/AgCl/Cl$^-$.

$$2H_2O + 2e^- \leftrightarrow H_2 + 2OH^- \qquad (4)$$

$$2H_2O \leftrightarrow O_2 + 4H^+ + 4e^- \qquad (5)$$

Within this window two redox systems are visible. The first cathodic peak is observed at -0.25 V vs Ag/AgCl/Cl$^-$, corresponding to the reduction of UO_2^{2+} to U^{4+}. A second cathodic peak appears at -0.50 V vs Ag/AgCl/Cl$^-$ and probably corresponds to the reduction of U^{4+} to U^{3+}.

Coupled anodic peaks expected for reversible one or two electron transfer processes are not observed in the oxidation cycle. The intensity of the reduction peak at -0.25 V vs Ag/AgCl/Cl$^-$ is proportional to the uranium concentration in the solution. The same system was also investigated with use of the separated anodic compartment and yielded similar results when using a high porosity glass frit (160 μm). The small porosity leads to an increase of the resistance but no significant change in the electrochemical signal was observed. The UO_2^{2+} system at 0.02 M, was also investigated at different pH's (from pH 1.1 to 2.2) with similar results obtained as in Fig. 3. As the reduction wave of to U^{4+} starts at -0.1 V vs Ag/AgCl/Cl$^-$, the electrolytic reduction of U(VI) to U(IV) was investigated with an applied potential of -0.300 V vs Ag/AgCl/Cl$^-$. The current varied in these experiments between 50 mA and 5 mA as the concentration of U(VI) diminished. The progress of reduction was monitored by cyclic voltammetry and by UV-Vis spectrophotometry. The conversion rate was calculated as the measured charge passed during the experiment divided by the theoretical charge required to reduce completely the U(VI) to U(IV) in the solution. Regardless of the initial concentration, the U(VI) solution was almost fully reduced. Fig. 4 shows results from cyclic voltammetry carried out occasionally during electrochemical reduction of a 0.1 M U solution.

The voltammograms show clearly the decrease of the cathodic UO_2^{2+}/U^{4+} reduction peak with increasing electrolysis time. UV-Vis absorption spectrophotometry (see Fig. 5) from the same experiment confirms these results. With the reduction of U(VI) to U(IV), the absorption bands of U(VI) at around 400 nm gradually
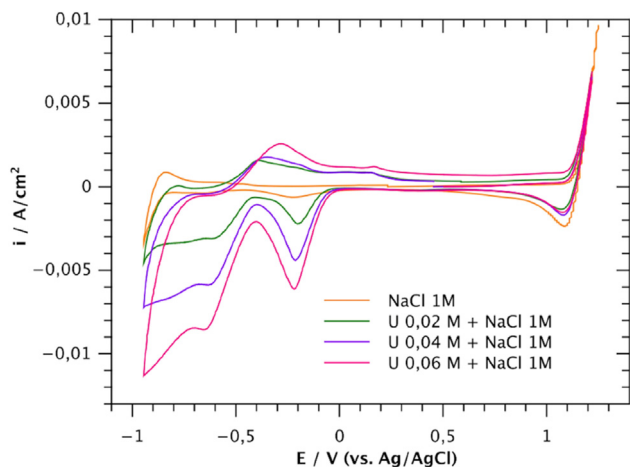
Fig. 4. Cyclic voltammetry during a reduction experiment, [U] $= 0.1$ M prepared from $UO_2(NO_3)_2$ in 0.33 M HCl at scan rate 0.1 V/s [24].

disappear and at the same time the typical absorption peaks for U(IV) at 426, 492, 548 and 646 nm appears, see Fig. 5. The intensity of the absorption peak of U(VI) at 412 nm decreases linearly with the theoretical conversion rate. During the reduction experiment the colour of the solution changed gradually from the typical uranyl yellow to green for U^{4+}.

The precipitation from electrochemically reduced U(IV) solutions, with concentrations up to 0.5 M U, was achieved by slow alkalinisation of the solution following as close as possible the theoretical solubility limit of U(IV). Black nc-UO_{2+x} precipitates normally appeared at pH < 1 and the solution appeared turbid from this point onwards. Fig. 6 shows the degree of precipitation with increasing pH, monitored by absorption spectrometry corresponding to remaining U(IV) in the solution. The concentration of U(IV) steadily decreased with increasing pH and the reaction is almost complete already at pH 1.6 which is in agreement with the theoretical solubility indicated in Fig. 1.

The morphology and structure of the obtained nc-UO_{2+x} particles were characterised by TEM and XRD. Fig. 7 shows the TEM image of the synthesised nc-UO_{2+x} precipitates at three different magnifications. The average precipitate size, obtained from TEM

Fig. 3. Cyclic voltammetry as a function of uranium concentration, $UO_2(NO_3)_2$ solutions in 1 M NaCl adjusted to pH = 3 at scan rate 0.1 V/s [24].
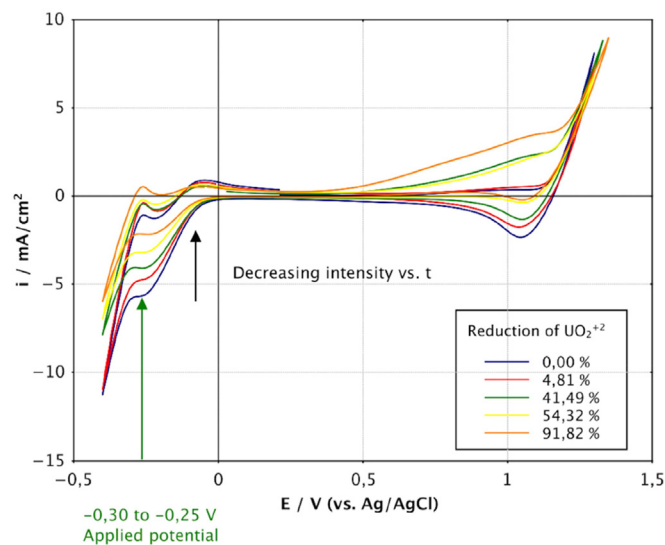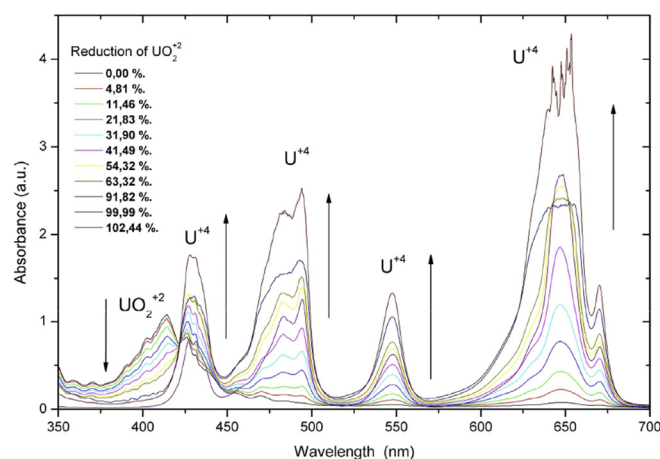
Fig. 5. Change in visible absorption spectra during the reduction experiment. Absorption peaks of U(VI) at 412 nm and of U(IV) are at 426, 492, 548 and 646 nm [24].
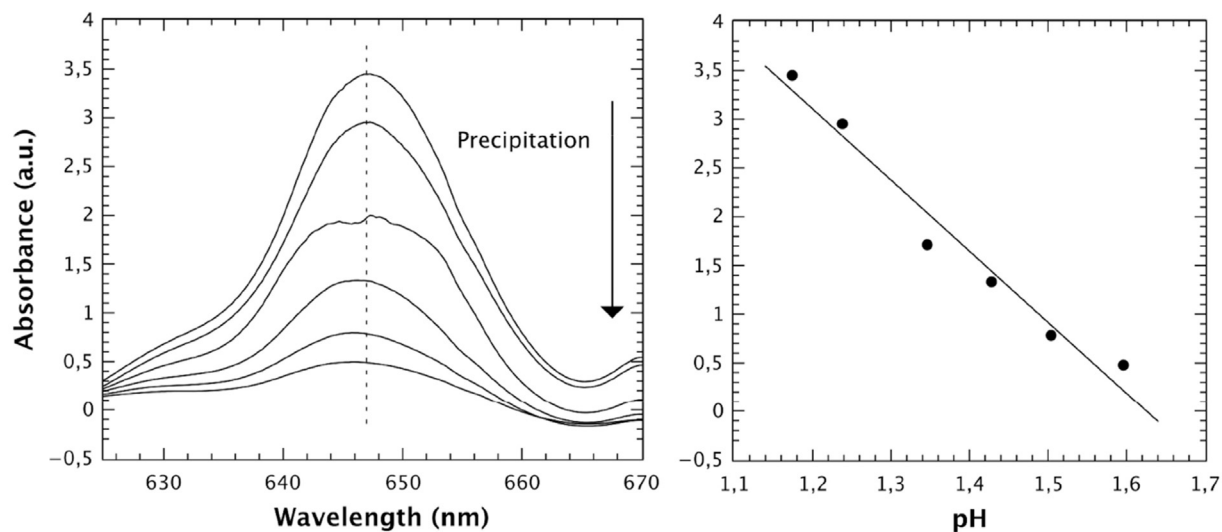
Fig. 6. Concentration decrease of U(IV) monitored by absorption spectrophotometry of the U(IV) peak at 646 nm during a typical precipitation experiment. Starting solution $[U^{4+}] = 0.1$ M, $[HCl] = 1$ M [24].
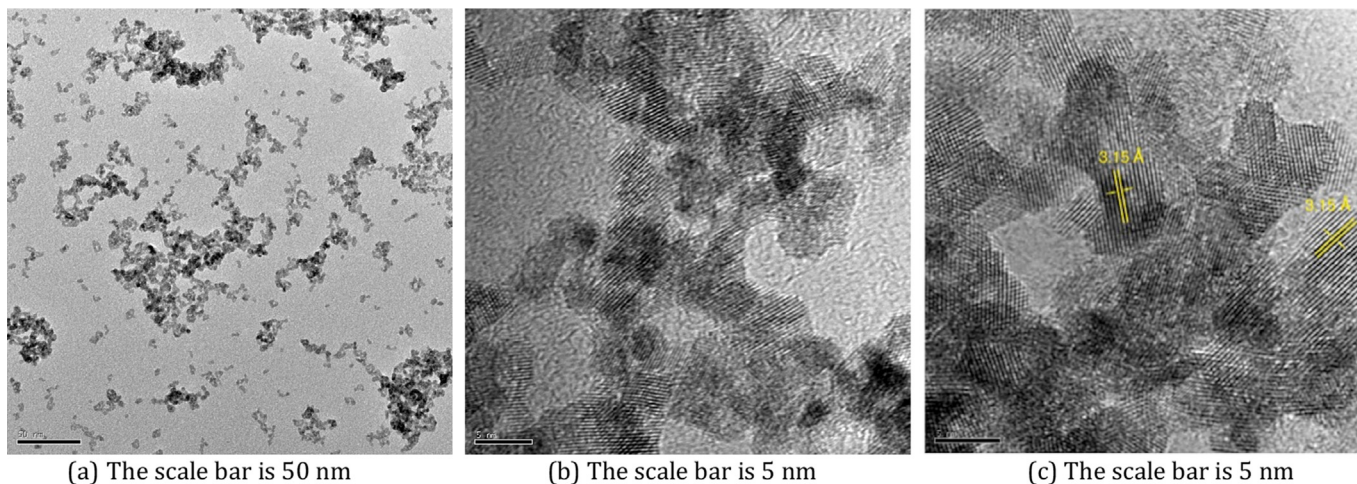

(a) The scale bar is 50 nm　　　　　　(b) The scale bar is 5 nm　　　　　　(c) The scale bar is 5 nm

Fig. 7. TEM micrographs of UO_2 at low resolution, showing an assembly of nanocrystals, and at high resolution, revealing lattice imaging of the nanocrystals [24].

imaging analysis, was 3.9 nm with a fairly narrow size distribution, as shown in Fig. 8.

The individual particles formed agglomerates with sizes up to 50 nm. The precipitates had the typical fcc fluorite structure of UO_2. The calculated interference fringe spacing in the HRTEM image, Fig. 7(c), is about 0.315 nm, which is in agreement with the interplanar distance of the [111] plane of the fcc fluorite structure for a reference fcc UO_2 standard (0.3153 nm, 00-041-1422-ICDD [25]).

The crystal structure measured in the HRTEM image was confirmed by Rietveld refinement of XRD measurements using a reference bulk fcc UO_2 as standard. The agreement between the measured and the fitted diffraction lines is shown in Fig. 9. The overall peak fitting quality, reached a weighted profile R-factor (Rwp) and a goodness of fit (GOF) of 5.39 and 1.51, respectively, which is satisfactory. A fcc fluorite structure (*Fm-3m* space group) with a lattice parameter of 0.5416 nm was determined which is close to the lattice parameter of the fcc UO_2 standard (0.547 nm): The crystallite size determined from XRD analysis was 3.8 nm and is in good agreement with 3.9 nm as obtained by TEM. The small shift to higher diffractions angles of the Bragg peaks, which suggests either a slightly higher oxidation state relative to stoichiometric
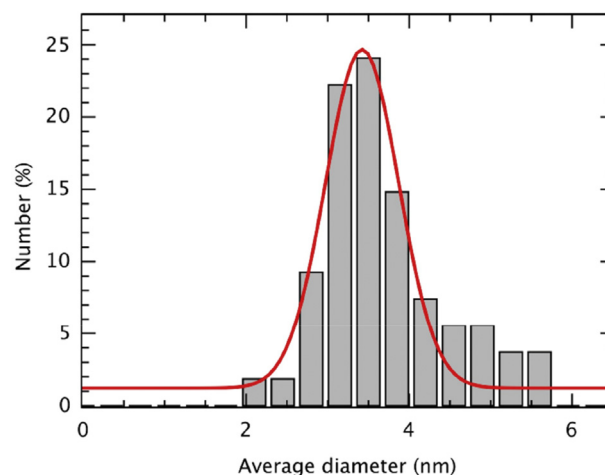

Fig. 8. Size distribution histogram as evaluated from TEM measurements of nc-UO_2 synthesised by controlled aqueous precipitation.
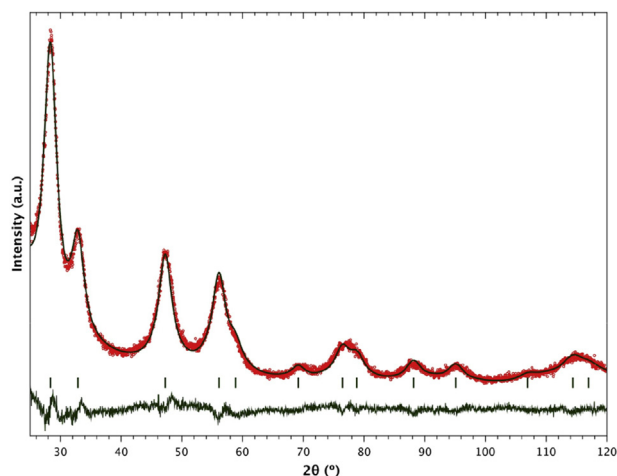
Fig. 9. Powder XRD pattern of nc-UO_{2+x} with black bars representing the calculated positions of the Bragg reflections of UO_2 (cubic Fm-$3m$). Red points, black line, and green line are corresponding to the observed pattern, calculated pattern and their difference respectively [24]. (For interpretation of the references to colour in this figure legend, the reader is referred to the web version of this article.)

Fig. 10. Bragg diffraction peak positions and relative intensities for the refined XRD pattern of nc-UO_{2+x} (green), standard UO_2 (00-041-1422-ICDD – red), U_4O_9 (04-005-4573-ICDD – blue) and U_3O_8 (00-023-1460-ICDD – lila), respectively [24,25]. (For interpretation of the references to colour in this figure legend, the reader is referred to the web version of this article.)
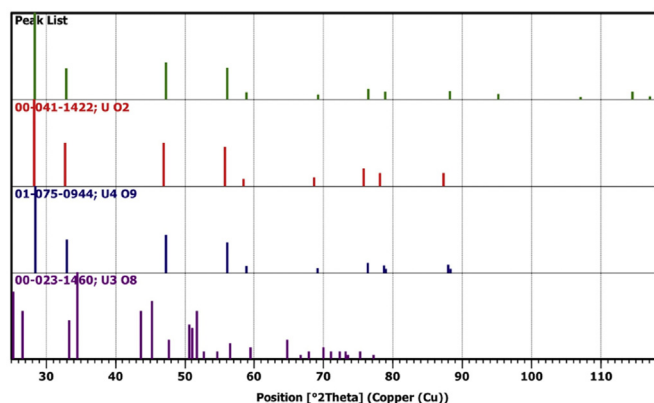
UO_2, or a mechanical distortion (contraction) of the lattice due to stresses induced by the small particle size [25–27].

The diffraction peak positions and relative intensities for the refined XRD patterns of the produced nc-UO_{2+x} nanocrystals in comparison with standard diffraction patterns of UO_2, U_4O_9 and U_3O_8, are shown in Fig. 10. The experimental peaks are compatible with an oxide structure in between those of fcc UO_2 and U_4O_9, but likely with an oxidation degree closer to that of U_4O_9. There is no evidence for a U_3O_8 phase in the nano particles at all.

The calculated interplanar distance of the [111] plane in the fcc fluorite structure was 0.3147 nm as derived from the XRD pattern shown in Fig. 9, which is compared to and 0.3153 nm for UO_2 (00-041-1422-ICDD), and 0.315 nm calculated for single crystals from HRTEM.

4. Conclusions

The electrochemical behaviour during the reduction of U(VI) to U(IV) in chloride solutions have been investigated using cyclic voltammetry. Different parameters such as the uranium concentration, pH and the use of a separated anodic compartment to avoid back reactions of the anodically produced oxygen were studied to define optimal electrolysis conditions. The characteristic reduction peak of U(VI) to U(IV) at around − 0.3 V vs Ag/AgCl/Cl⁻ was proportional to the uranium concentration and insensitive to changes in pH, indicating the feasibility to use higher uranium concentrations with correspondingly lower pH's in a conversion process of U(VI) to U(IV) by electrolysis. The reduction of U(VI) to U(IV) during electrolysis was monitored by absorption spectrophotometry and could be correlated to the intensity of the reduction peak in cyclic voltammetry.

Precipitation from electrolytically reduced U(IV) solutions was achieved by slow and controlled alkalinisation following as close as possible the theoretical solubility limit line of U(IV) in aqueous media. Nano-crystalline UO_{2+x} precipitation occurred in the pH range from about 1 to 3 and for a uranium concentration as high as 0.5 M. Washing steps with combined centrifugation of the dark solution yielded nc-UO_{2+x} precipitates essentially free from solutions components. As a result, nc-UO_{2+x} productions in the range of 10 g per batch were obtained. This represents not only an improvement of the method studied but a major achievement in its use for the synthesis of meaningful quantities of such material.

The black solid phase crystallised with the typical UO_2-fcc fluorite structure (Fm-$3m$ space group) with a lattice parameter a = 0.5416 nm and an average crystallite size of 3.8 nm, in agreement with the average size obtained by TEM (3.9 nm). The predominant diffraction features of the samples corresponded unmistakably to UO_2, accompanied by a peak broadening characteristic of finely aggregated nc-particles, just as observed by TEM. This phase has been previously described in the literature as amorphous −hydrated uraninite and was shown in this work to correspond to crystalline UO_2 but in a slightly oxidised state.

Acknowledgements

Appendix A. Supplementary data

Supplementary data related to this article can be found at http://dx.doi.org/10.1016/j.jnucmat.2016.04.050.

References

[1] F. Garzarolli, R. von Jan, H. Stehle, The main causes of fuel failure in water cooled power reactors, At. Energy Rev. 17 (1) (1979) 31–128.
[2] M. Watteau, B. Estève, R. Güldner, R. Hoffman, Framatome ANP extended burnup experience and views on LWR fuels, in: World Nuclear Association, Annual Symposium, 2001.
[3] H. Matzke, J. Spino, Formation of the rim structure in high burnup fuel, J. Nucl. Mater. 248 (0) (1997) 170–179.
[4] J. Spino, D. Papaioannou, Lattice parameter changes associated with the rim-structure formation in high burn-up UO_2 fuels by micro X-ray diffraction, J. Nucl. Mater. 281 (2–3) (2000) 146–162.
[5] J. Noirot, L. Desgranges, J. Lamontagne, Detailed characterisations of high burn-up structures in oxide fuels, J. Nucl. Mater. 372 (2–3) (2008) 318–339.
[6] J. Spino, D. Papaioannou, J.-P. Glatz, Comments on the threshold porosity for fission gas release in high burn-up fuels, J. Nucl. Mater. 328 (1) (2004) 67–70.
[7] J.-P. Hiernaut, T. Wiss, J.-Y. Colle, H. Thiele, C.T. Walker, W. Goll, R.J.M. Konings, Fission product release and microstructure changes during laboratory annealing of a very high burn-up fuel specimen, J. Nucl. Mater. 377 (2) (2008) 313–324.
[8] T.E. Chung, T.J. Davies, The superplastic creep of uranium dioxide, J. Nucl. Mater. 79 (1) (1979) 143–153.
[9] J. Spino, H.S. Cruz, R. Birtcher, C. Ferrero, R. Pierritz, A. Fernández,

Developments at ITU towards a high-performance, gas-retentive and PCI-resistant nanocrystalline UO$_2$-fuel, in: Workshop on Radiation Stability of Complex Microstructures. Santa Fe, USA, 2008.

[10] J. Spino, H. Santa-Cruz, R. Jovani-Abril, R. Birtcher, C. Ferrero, Bulk-nano-crystalline oxide nuclear fuels — an innovative material option for increasing fission gas retention, plasticity and radiation-tolerance, J. Nucl. Mater. 422 (1–3) (2012) 27–44.

[11] K. Opel, S. Weiß, S. Hübener, H. Zänker, G. Bernhard, Study of the solubility of amorphous and crystalline uranium dioxide by combined spectroscopic methods, Radiochim. Acta 95 (3) (2007) 143–149.

[12] G. Rousseau, M. Fattahi, B. Grambow, F. Boucher, G. Ouvrard, Coprecipitation of thorium with UO$_2$, Radiochim. Acta 90 (9–11) (2002) 523–527.

[13] G. Rousseau, M. Fattahi, B. Grambow, F. Boucher, G. Ouvrard, Coprecipitation of thorium and lanthanum with UO$_{2+x(s)}$ as host phase, Radiochim. Acta 94 (9–11) (2006) 517–522.

[14] G. Rousseau, M. Fattahi, B. Grambow, L. Desgranges, F. Boucher, G. Ouvrard, N. Millot, J.C. Nièpce, Synthesis and characterization of nanometric powders of UO$_{2+x}$, (Th,U)O$_{2+x}$ and (La,U)O$_{2+x}$, J. Solid State Chem. 182 (10) (2009) 2591–2597.

[15] Q. Wang, G.-D. Li, S. Xu, J.-X. Li, J.-S. Chen, Synthesis of uranium oxide nanoparticles and their catalytic performance for benzyl alcohol conversion to benzaldehyde, J. Mater. Chem. 18 (10) (2008) 1146–1152.

[16] H. Wu, Y. Yang, Y.C. Cao, Synthesis of colloidal uranium–dioxide nanocrystals, J. Am. Chem. Soc. 128 (51) (2006) 16522–16523.

[17] D. Hudry, C. Apostolidis, O. Walter, T. Gouder, E. Courtois, C. Kübel, D. Meyer, Non-aqueous synthesis of isotropic and anisotropic actinide oxide nano-crystals, Chem. A Eur. J. 18 (27) (2012) 8283–8287.

[18] D. Gil, R. Malmbeck, J. Spino, Th. Fanghänel, R.E. Dinnebier, Nanoscale UO$_2$ and novel complex U(IV)-sulphate phase formation from electrolytically reduced uranyl sulphate solutions, Radiochim. Acta 98 (2) (2010) 89.

[19] V. Neck, J.I. Kim, Solubility and hydrolysis of tetravalent actinides, Radiochim. Acta (2001) 89.

[20] T. Fanghänel, V. Neck, Aquatic chemistry and solubility phenomena of actinide oxi-des/hydroxides, Pure Appl. Chem. 74 (10) (2002) 1895–1907.

[21] D. Rai, M. Yui, D.A. Moore, Solubility and solubility product at 22°C of UO$_2$(c) precipitated from aqueous U(IV) solutions, J. Solut. Chem. 32 (1) (2003) 1–17.

[22] K. Fujiwara, H. Yamana, T. Fujii, H. Moriyama, Determination of uranium(IV) hydrolysis constants and solubility product of UO$_2$·xH$_2$O, Radiochim. Acta 91 (6) (2003) 345–350.

[23] K. Fujiwara, H. Yamana, T. Fujii, K. Kawamoto, T. Sasaki, H. Moriyama, Solubility product of hexavalent uranium hydrous oxide, J. Nucl. Sci. Technol. 42 (3) (2005) 289–294.

[24] R. Jovani-Abril, Synthesis and Characterization of Nanocrystalline UO$_2$ ceramics, Universidad de Santiago de Compostela (USC), 2014.

[25] ICDD, The International Centre for Diffraction Data [Online], 2012, www.icdd.com.

[26] W.H. Qi, M.P. Wang, Y.C. Su, Size effect on the lattice parameters of nano-particles, J. Mater. Sci. Lett. 21 (11) (2002) 877–878.

[27] M. Fukuhara, Lattice expansion of nanoscale compound particles, Phys. Lett. A 313 (5–6) (2003) 427–430.